NANOSYSTEMS:
PHYSICS, CHEMISTRY, MATHEMATICS

Original article

Sozarukova M.M., et al. *Nanosystems: Phys. Chem. Math.*, 2025, **16** (6), 791–801.
http://nanojournal.ifmo.ru
DOI 10.17586/2220-8054-2025-16-6-791-801

UV-tuning the redox properties of nanoscale cerium dioxide and its enzyme conjugates

Madina M. Sozarukova[1,a], Arina D. Filippova[1,b], Daria-Maria V. Ratova[2,c], Ivan V. Mikheev[2,d], Elena V. Proskurnina[1,e], Alexander E. Baranchikov[1,f], Vladimir K. Ivanov[1,g]

[1]Kurnakov Institute of General and Inorganic Chemistry of the Russian Academy of Sciences, Moscow, Russia
[2]Analytical Chemistry Division, Chemistry Department, M. V. Lomonosov Moscow State University, Moscow, Russia

[a]s_madinam@bk.ru, [b]arifilippova@yandex.ru, [c]darmarrat@gmail.com, [d]mikheev.ivan@gmail.com, [e]proskurnina@gmail.com, [f]a.baranchikov@yandex.ru, [g]van@igic.ras.ru

Corresponding author: Vladimir K. Ivanov, van@igic.ras.ru

PACS 61.46.+w, 82.50.Hp, 82.70.Dd, 87.14.Ee

ABSTRACT This study investigated the redox properties of cerium oxide nanoparticles (CeO_2 NPs) and their conjugates with superoxide dismutase (SOD) or horseradish peroxidase (HRP) as well as the UV-induced modulation of these properties. UV exposure non-monotonically decreased the SOD-like property of the bare CeO_2 NPs. The CeO_2 conjugates with enzymes were analyzed both immediately after preparation and after being aged for 3 h. Chemiluminescence assays showed the synergistic effect for the CeO_2-SOD conjugates which showed high SOD activity. Additionally, CeO_2 NPs enhanced the stability of the conjugated SOD under UV exposure thus demonstrating a photoprotective function. The CeO_2-HRP conjugates demonstrated lower prooxidant activity compared to the bare enzyme, however higher stability under UV irradiation. The effect of UV radiation on CeO_2-HRP conjugates was found to be multidirectional and depended on the incubation time of the CeO_2 NPs with the enzyme. The results demonstrated that CeO_2-enzyme conjugates offer tunable dual functionality and UV light could be an important parameter affecting their redox properties. The latter effect should be taken into account for designing advanced cosmeceutical formulations.

KEYWORDS nanoceria, superoxide dismutase, peroxidase, UV irradiation, enzyme, conjugate, redox modulation, photoprotection

ACKNOWLEDGEMENTS This study was supported by the Russian Science Foundation (Project no. 24-13-00370).

FOR CITATION Sozarukova M.M., Filippova A.D., Ratova D.-M.V., Mikheev I.V., Proskurnina E.V., Baranchikov A.E., Ivanov V.K. UV-tuning the redox properties of nanoscale cerium dioxide and its enzyme conjugates. *Nanosystems: Phys. Chem. Math.*, 2025, **16** (6), 791–801.

1. Introduction

Cerium dioxide nanoparticles (CeO_2 NPs) are now regarded as one of the most promising next-generation biomimetic agents. Their appeal stems from a unique combination of physicochemical properties and a broad range of enzyme-mimetic activities [1–3]. Significant research efforts are now directed toward engineered hybrid organic-inorganic materials that allow modulating the properties of nanoscale cerium dioxide using various biocompatible compounds including proteins, enzymes, amino acids, etc. [4–10]. The immobilization of biologically active molecules on the surface of CeO_2 NPs provides a functional platform for the targeted delivery of drugs and various bioactive ligands, as well as enhancing therapeutic efficacy through synergistic interactions and prolonged activity [11, 12].

Reactive oxygen species (ROS) such as the superoxide anion radical ($\cdot O_2^-$) and hydrogen peroxide, are essential for normal physiological functions [13, 14]. In living systems, they play a crucial role in maintaining homeostasis and facilitating cellular signaling. However, their overproduction can result in a cellular damage by inducing oxidative stress. Living systems counteracts oxidative stress through production of antioxidants, e.g. enzymes, such as superoxide dismutase (SOD), catalase, glutathione peroxidase, etc. Notably, SOD plays a critical role by regulating the balance between intracellular oxidative processes and antioxidant defense system [15].

The ability of nanoscale cerium dioxide to mimic SOD was among the first enzyme-like properties discovered for CeO_2 NPs [16–19]. It is well established that the SOD-like activity of CeO_2 NPs depends on a multitude of factors. These include synthesis conditions [20], redox state of surface cerium atoms [16, 17, 21], particle size and shape [19, 22, 23], surface functionalization [24–26]. The SOD-like activity depends also on the presence of phosphate species [27],

pH [19, 28, 29], temperature [30], etc. To enhance the catalytic activity, hybrid materials are being created based on cerium dioxide conjugated with antioxidant and prooxidant enzymes, such as SOD, catalase, and peroxidase [5, 22, 31]. Interestingly, the dismutation of superoxide anion radicals catalyzed by both native SOD or SOD mimetics though results in a pronounced antioxidant outcome, however it simultaneously leads to the accumulation of hydrogen peroxide being another type of ROS.

Despite the significant progress in understanding the biocatalytic properties of CeO_2 NPs and their hybrids with biomolecules, the ability to control their redox activity using external physical factors remains underexplored. In this context, ultraviolet (UV) radiation is of particular interest [32, 33]. As a potent exogenous agent, UV radiation serves not only as a convenient tool for controlled exposure but also as a physical model of oxidative stress [34]. The mechanism of UV-action on living systems is multifactorial involving both the production of free radicals and direct damage of biomolecules [35, 36].

The surface properties of cerium dioxide which is a wide-bandgap semiconductor, can be modified upon exposure to ultraviolet light. These changes can involve the alterations of its surface hydroxylation [37]. An example of a similar phenomenon is titanium dioxide (TiO_2), which exhibits UV-induced superhydrophilicity [38, 39]. Given that the enzyme-like properties of nanoscale cerium dioxide are largely governed by surface chemistry, UV irradiation is hypothesized to be an effective tool for modulating the catalytic activity of CeO_2 NPs. However, the effects of UV irradiation on the redox activity of both bare CeO_2 NPs and their enzyme conjugates remain virtually unexplored. Specifically, the UV-modulation of their interaction with key cellular enzymes, such as superoxide dismutase and peroxidase, by UV exposure has not been assessed.

This study provides an investigation of the effects of UV irradiation on the redox activity of bare CeO_2 NPs and their conjugates with enzymes. The activity was assessed towards key reactive oxygen species – the superoxide anion radicals and hydrogen peroxide – by the chemiluminescence method. The CeO_2 conjugates were studied with different oxidoreductase enzymes, superoxide dismutase or horseradish peroxidase (HRP). For the first time, it was shown that UV irradiation can not only suppress, but selectively and dose-dependently modulate the enzyme-like activity of nanoparticles. The findings of this study demonstrate the significant potential of nanoscale cerium dioxide for application in advanced cosmetic preparations.

2. Materials and methods

2.1. Materials (chemicals)

The following reagents were used in this work: ammonium cerium(IV) nitrate ($(NH_4)_2[Ce(NO_3)_6]$, chem. pure, Lankhit), isopropanol (high purity, Aldosa), superoxide dismutase from bovine erythrocytes (Cu/Zn type, ≥ 97 % , S7446-15KU, Sigma-Aldrich), horseradish peroxidase (RZ> 1.0, $a \geq 110$ U/mg, DIA-M).

2.2. Synthesis of bare CeO_2 nanoparticles and preparation of ceria-enzyme conjugates

Bare CeO_2 nanoparticles were prepared by thermohydrolysis of an aqueous ammonium cerium(IV) nitrate solution, following a reported procedure [40]. Briefly, cerium salt (2.33 g) was dissolved in 23 mL of water. The resulting solution (0.185 M) was maintained at 95 °C for 24 h. Following centrifugation to isolate the yellow precipitate from the mother liquor, the product was washed three times with isopropyl alcohol and redispersed in deionized water. Finally, the sol was boiled for 3 h to eliminate isopropanol residuals.

Cerium dioxide was functionalized with two enzymes: superoxide dismutase (CeO_2-SOD conjugate) and horseradish peroxidase (CeO_2-HRP conjugate). The functionalization was performed by gradually adding the CeO_2 sol to an aqueous solution of the enzyme. This process achieved a final molar ratio CeO_2 : enzyme 10000 : 1. Two types of CeO_2 conjugates with SOD and HRP were analyzed: as prepared (0 h pre-incubation) and incubated under stirring for 3 h. All the samples were stored in dark. For physicochemical characterization, the enzyme-conjugated CeO_2 sols were dried at 25 °C.

2.3. Materials characterization

The concentration of the initial ligand-free cerium dioxide sol was determined gravimetrically.

The X-ray powder diffraction analysis (XRD) of ceria samples was performed using a Bruker (Billerica, MA, USA) D8 Advance diffractometer (CuKα radiation). Data were collected over a 2θ range of 20 – 100° with a step size of 0.02° and a counting time of 0.2 seconds per step. Phase identification was performed using the ICDD PDF2 database. The crystallite size (coherent scattering domain size) was estimated using the Scherrer equation; peak profiles were fitted to pseudo-Voigt functions.

The optical absorption spectra were recorded in quartz cuvettes using an SF-2000 spectrophotometer (Spectr, Saint Petersburg, Russia). Measurements were conducted in the range of 200 – 600 nm with a 1 nm step size.

Fourier transform infrared (FTIR) spectra were obtained on an InfraLUM FT-08 spectrometer (Russia) employing the attenuated total reflection (ATR) technique. Spectra were recorded in the 400 – 4000 cm^{-1} range with a spectral resolution of 1 cm^{-1}.

Dynamic light scattering (DLS) and zeta potential measurements were performed at 20 °C and at 36 °C using a Photocor Compact-Z analyser (Photocor, Moscow, Russia). The correlation function for each sample was collected by averaging 10 individual 20 sec runs. The hydrodynamic diameter of the particles was determined using a regularization algorithm (DynalS software).

2.4. UV-exposure procedure

The samples (absorbance ≤ 0.2, $V = 2$ ml) were irradiated in glass vessels (5 ml) using a Bio-Link UV irradiation system (Vilber Lourmat, Collégien, France) at 312 nm (UV source 5×8-watt lamps). The samples were irradiated with doses of 50 or 100 mJ/cm^2. The samples were irradiated from above, the height of liquid sample was approximately 3 cm.

2.5. Analysis of SOD-like activity

The SOD-like activity of the materials was analyzed using a method based on the detection of lucigenin chemiluminescence during its oxidation by superoxide anion radicals ($\cdot O_2^-$). The superoxide anion radicals are generated by the oxidation of xanthine to uric acid in the presence of oxygen [41, 42].

Aliquots of aqueous solutions of xanthine (20 μM, #X0626, Sigma), lucigenin (20 μM, #393824, J&K, San Jose, CA, USA), and the test sample were rapidly added into a cuvette containing a phosphate buffer solution (100 mM, pH 7.4). The background signal was recorded for 30 – 60 s, then xanthine oxidase ($a = 8.8$ mU/mL, #X1875-25UN, Sigma) was added. All experiments were conducted in triplicate. The chemiluminescence intensity was measured at 37 °C using a Lum-1200 (DISoft, Moscow, Russia) 12-channel chemiluminometer. The results were processed using the PowerGraph software (version 3.3).

2.6. Analysis of prooxidant activity

The prooxidant activity of the materials was analyzed towards hydrogen peroxide in the presence of luminol (5-amino-1,2,3,4-tetrahydro-1,4-phthalazinedione, 3-aminophthalic acid hydrazide) [31, 43].

Aliquots of H_2O_2 (10 mM, #H1009, Sigma) and luminol (50 μM, #A8511, Sigma) were rapidly introduced into a cuvette containing phosphate buffer solution (100 mM, pH 7.4). The background signal was recorded for 60 – 90 s. After the chemiluminescence intensity reached a constant value, an aliquot of the test sample was added. All experiments were conducted in triplicate. Chemiluminescence was measured using a Lum-1200 (DISoft, Moscow, Russia) 12-channel chemiluminometer. The results were processed using PowerGraph software (version 3.3).

3. Results and discussion

3.1. Characterisation of CeO_2-based nanomaterials

Powder X-ray diffraction analysis (XRD) revealed that the crystalline phase in the bare CeO_2 sol and CeO_2 conjugates with SOD and HRP enzymes corresponded to single-phase cerium dioxide (space group $Fm\bar{3}m$, PDF2 00-034-0394) (Fig. 1(a)). The cerium dioxide crystallite size (~ 2.8 nm) remains virtually unchanged after enzyme immobilization.

UV-visible spectroscopy revealed an absorption band between 280 – 300 nm for the enzyme-modified ceria sols (Fig. 1(b)), which is characteristic of nanoscale CeO_2 with a band gap of 3.3 eV. The modified ceria sols show no absorption band at ~ 250 nm. This band corresponds to the $4f^1 \rightarrow 5d^1$ transition of Ce^{3+}. Therefore, Ce^{4+} was not reduced to Ce^{3+} during the functionalization of CeO_2 with enzymes.

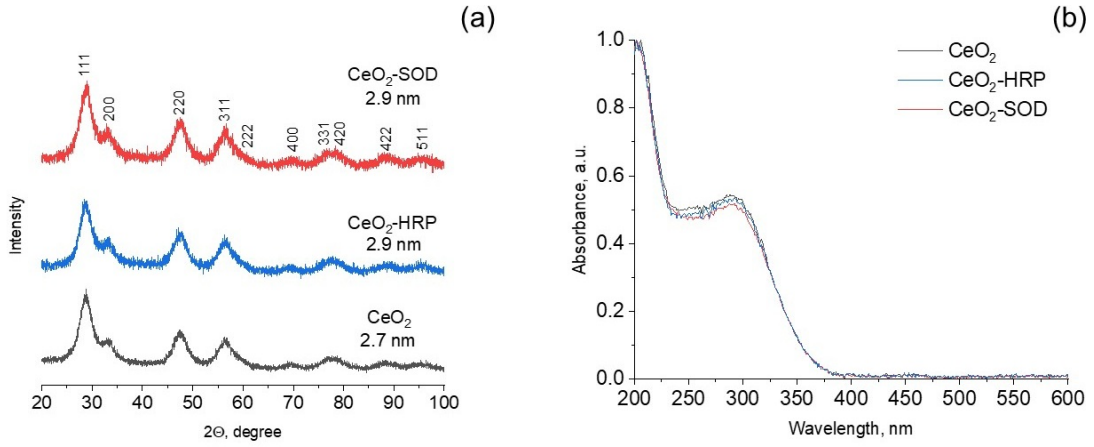

FIG. 1. (a) X-ray diffraction patterns of bare CeO_2 NPs and ceria conjugates with SOD and HRP; (b) electron absorption spectra of CeO_2-based nanomaterials

The ceria sols were characterized by DLS at 20 and 36 °C, these temperatures correspond to sample storage and chemiluminescence measurement conditions, respectively (Fig. 2). The unstabilized CeO_2 sol exhibited a nearly monodisperse particle size distribution with a mean diameter of 14 nm and a minor fraction of larger agglomerates (~ 140 nm). Modification of the nanoscale CeO_2 with SOD did not induce significant changes in the particle size distribution; the mean aggregate diameter remained at 15 – 16 nm (Fig. 2(a,b)). In contrast, modification with HRP induced some changes, and the formation of two aggregate fractions with sizes of 11 and 27 nm was registered (Fig. 2(a,b)). Fig. 2(c) shows the particle size distribution in the aqueous solutions of the bare enzymes. The SOD solution contains three particle fractions with average hydrodynamic diameters of 3, 24, and 270 nm. Similarly, three distinct fractions with average sizes of 4, 60, and 430 nm were identified in the HRP solution. It is important to note that the enzyme concentrations (superoxide dismutase and horseradish peroxidase) in the modified ceria sols were 1 μM, which is 30 times lower than the enzyme concentration in their individual solutions (30 μM). At such low concentrations, the contribution of the bare enzymes to light scattering of the CeO_2 conjugates could be regarded as negligible.

Electrokinetic measurements revealed that modification of CeO_2 NPs with enzymes significantly changed their electrical properties. A notable increase in ζ-potential was observed, rising from $+25$ mV for the bare CeO_2 NPs to $+33$ mV for the CeO_2-SOD conjugate and to $+36$ mV for the CeO_2-HRP conjugate. This increase in ζ-potential indicates enhanced colloidal stability of the modified nanoparticles. Interestingly, this finding is somewhat counterintuitive as the enzyme-modified ceria sols possessed higher pH (4.5 for CeO_2-SOD and 5.6 for CeO_2-HRP) than that of the bare CeO_2 sol (pH 2.1) and thus a decrease in the absolute ζ-potential value could be expected [44]. However, the observed change in ζ-potential value supports well the successful immobilization of enzymes on the surface of the CeO_2 NPs. In the recent report, the hemolymph serum of *Mytilus galloprovincialis* was shown to form a protein corona on the surface of commercial CeO_2 NPs [45]. The corona consisted of SOD and shifted the ζ-potential value of the NPs from a highly negative -84 mV to -10 mV.

The ceria sols were analyzed by DLS after one month of storage in a dark environment at 4 – 8 °C. The unmodified CeO_2 sol showed no change in its primary particle size (13 nm), but its larger agglomerates shrank by more than half, to 63 nm (Fig. 2(a,d)). The CeO_2 sol modified with SOD exhibited three distinct particle sizes: 14, 65, and 350 nm (Fig. 2(d)). The size of the key particle fraction in the CeO_2-SOD conjugate (14 nm) remained stable during storage. Notably, ceria sol modified with HRP had a more uniform particle size distribution after storage, with average sizes of 15 and 100 nm (Fig. 2(d)).

The DLS method was also used to investigate the aggregation behavior of CeO_2 particles in the sols after UV irradiation. For the experiment, two UV doses were chosen, 50 mJ/cm^2 and a higher dose of 100 mJ/cm^2. Exposure to a low-dose UV radiation (50 mJ/cm^2) resulted in a slight broadening of the particle size distributions in all the sols. However, the overall profile of the size distributions and the average aggregate sizes remained unchanged (Fig. 2(a,e)). In contrast, exposure to the higher UV dose (500 mJ/cm^2) induced significant aggregation of the particles. Specifically, in the CeO_2-HRP conjugate the average aggregate size doubled to 30 nm, and the presence of larger agglomerates up to 550 nm was observed (Fig. 2(a,f)).

The FTIR spectra of bare CeO_2 NPs, enzymes, and the conjugates are shown in Fig. 3.

In the IR spectra of cerium dioxide, the broad bands at 3600 – 3100 cm^{-1} and 3200 – 2500 cm^{-1} correspond to the O–H stretching vibrations of adsorbed water and the stretching vibrations of surface hydroxyl groups, respectively [46]. The determination of absorption bands of the protein carbon backbone or amide groups is challenging due to overlapping with the strong water absorption bands. Nevertheless, the spectra of HRP and SOD reveal several weak bands in the 3000 – 2840 cm^{-1} range (ν(C–H)) and a band at 3270 cm^{-1} (ν(N–H) of secondary amides) [47]. A band in the 1570 – 1515 cm^{-1} range, attributed to N–H bending vibrations of secondary amides (amide II), is observed in the spectra of both the bare enzymes and their conjugates with CeO_2. Bands characteristic of –CH_2– deformation vibrations were registered in the 1470 – 1400 cm^{-1} range. The absorption band for the C=O stretching vibration (amide I) is $\sim$10 cm^{-1} redshifted in the IR spectra of the CeO_2-SOD (1626 cm^{-1}) and CeO_2-HRP (1626 cm^{-1}) conjugates relative to the bare enzymes (1635 and 1638 cm^{-1}). These shifts support the successful formation of CeO_2-enzyme conjugates by indicating the interaction between the nanoparticles and the proteins.

3.2. Chemiluminescence assay

3.2.1. SOD-like activity. Analysis of the SOD-like activity was performed by monitoring chemiluminescence in the presence of lucigenin, a selective probe for superoxide anion radical generation [41, 42].

The effect of UV irradiation was investigated on the redox behavior towards the superoxide anion radicals $\cdot O_2^-$ of bare CeO_2 NPs, SOD enzyme, and CeO_2-SOD conjugates immediately after the mixing of components and incubated for 3 h. Fig. 4(a) shows experimental chemiluminescence curves recorded upon the addition of xanthine oxidase to the mixtures containing xanthine, lucigenin, and the analysed materials. These curves were recorded for the samples which were not subjected to UV-irradiation, or the UV-irradiated samples. As can be seen, in the presence of the analysed materials a decrease in lucigenin-dependent chemiluminescence is observed. The decrease in the chemiluminescence intensity is proportional to the concentration of superoxide anion radicals and could be used to quantify the SOD-like activity.

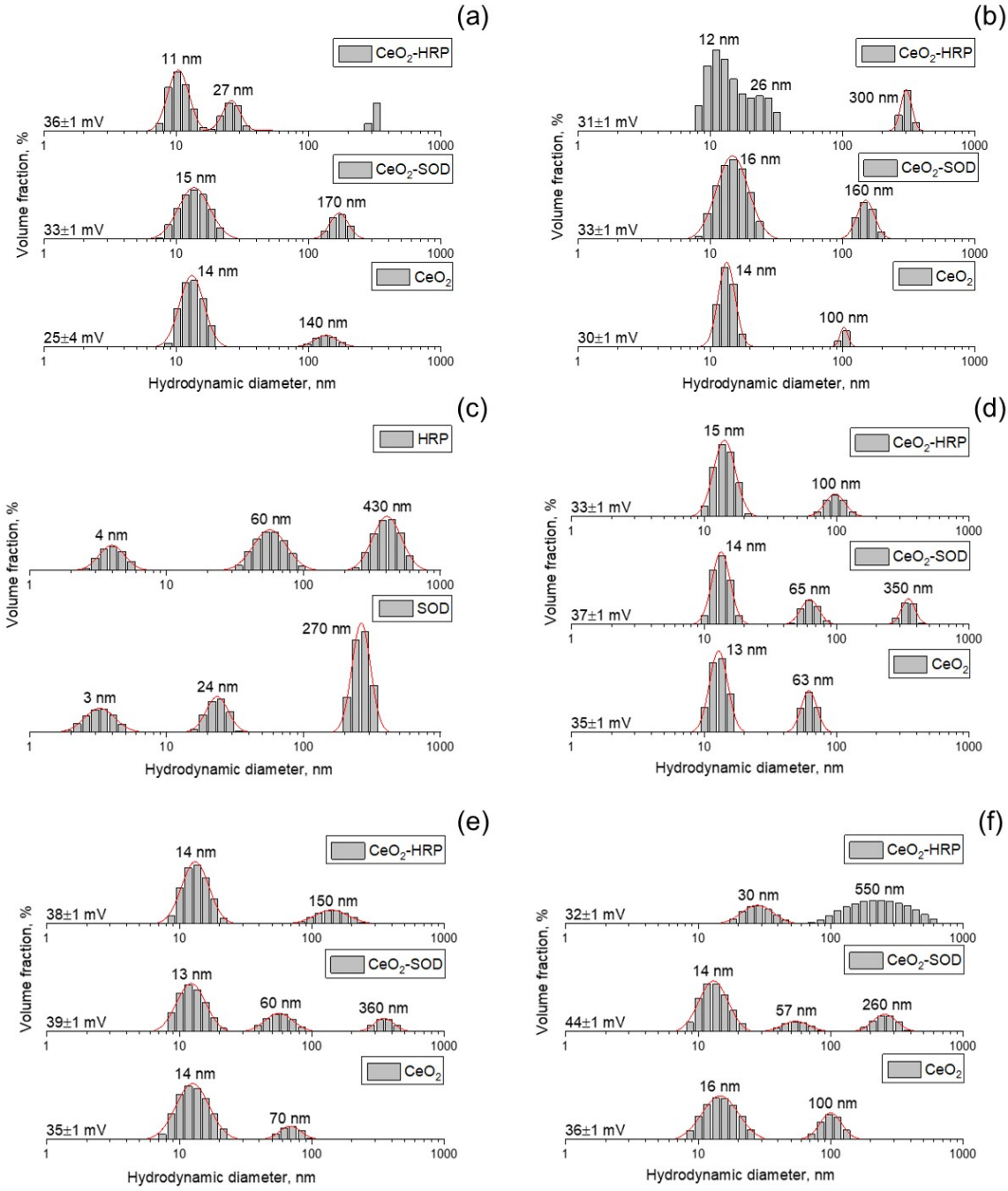

FIG. 2. Hydrodynamic diameter distributions for particles in unmodified CeO_2 sol (pH 2.1) and CeO_2 sols modified with SOD (pH 4.5) and HRP (pH 5.6), measured at (a) 20 °C and (b) 36 °C; (c) hydrodynamic diameter distributions in the solutions of the individual SOD and HRP enzymes (20 °C); (d) hydrodynamic diameter distributions in ceria sols after 1 month of storage (20 °C); hydrodynamic diameter distributions after UV irradiation of ceria sols with doses of (e) 50 mJ/cm^2 and (f) 100 mJ/cm^2 (20 °C)

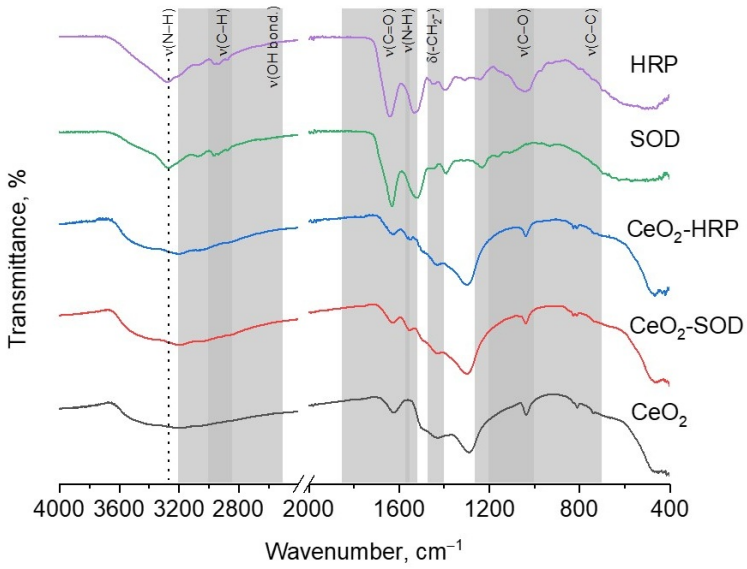

FIG. 3. FTIR spectra of bare CeO_2 NPs, individual enzymes SOD and HRP and conjugates of CeO_2 with enzymes

To quantify the SOD-like activity, the relative degree of chemiluminescence suppression, $\Delta S_{\text{rel.}}$, was calculated from the chemiluminograms (Fig. 4(b)) using the relation:

$$\Delta S_{\text{rel.}},\ \% \ = \ \frac{(S_0 \ - \ S)}{S_0} \times 100\%, \tag{1}$$

where S_0 and S are the light sums (integral intensity) for the control experiment (without the addition of sample) and for the experiment with the analysed sample.

The CeO_2-SOD conjugates showed nearly 2.5 times higher efficacy in scavenging superoxide anion radicals than bare CeO_2 NPs and 1.5 times higher efficacy than SOD enzyme (Fig. 4(b)). This observation can be attributed to the synergistic interactions between the components [5, 20, 31].

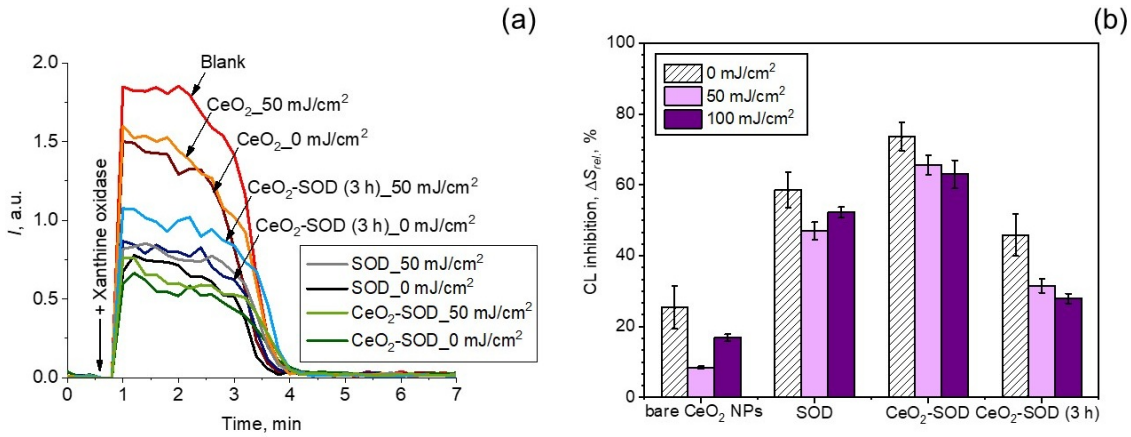

FIG. 4. (a) Chemiluminograms illustrating the SOD-like activity of bare CeO_2 NPs, bare SOD and CeO_2-SOD conjugates, (b) histograms of the relative degree of chemiluminescence suppression ($\Delta S_{\text{rel.}}$) for the samples

The effect of UV irradiation on the SOD-like activity of bare CeO_2 NPs is multidirectional. Exposure to a dose of 50 mJ/cm^2 suppressed the activity approximately threefold. Conversely, a higher dose of 100 mJ/cm^2 produced a weaker effect, the activity reduced by one and a half times (Fig. 4(b)). This indicates that the SOD-like activity of bare CeO_2 NPs can be modulated by UV exposure. The observed non-linear response for bare CeO_2 NPs to UV irradiation could be discussed in terms of photochemistry of oxide semiconductors, e.g. TiO_2 [38, 39, 48]. In particular, this effect can be due to the competition between the surface photooxidation (resulting in surface passivation) at low doses and the photoreduction (resulting in surface activation) at high doses. These competing processes can affect the surface hydroxylation of nanoscale cerium oxide which is expected to govern its enzyme-like activity [37]. A dose of 50 mJ/cm^2

presumably promotes the oxidation and desorption of surface hydroxyl groups, while a higher dose of 100 mJ/cm^2 induces the photoreduction of surface Ce^{4+} cations and facilitates surface re-hydroxylation. Recently, the UV exposure has been shown to increase the concentration of subvalent Ce^{3+} ions in parallel with a rise in the catalytic activity of CeO_2 NPs [49]. Thus, UV irradiation has been regarded as a novel strategy for modulating the catalytic activity of nanoscale ceria through annealing-free defect engineering [49].

UV irradiation was found to suppress the SOD-like activity of both SOD enzyme and the CeO_2-SOD conjugates (Fig. 4(b)). The UV-induced decrease in the activity is summarized in Table 1. These data are also illustrated in Fig. 5.

TABLE 1. Effects of UV irradiation on SOD-like activity of the samples.

Dose, mJ/cm^2	50	100
Sample	Reduction of SOD-like activity under UV irradiation, %	
Bare CeO_2 NPs	67 ± 7	34 ± 9
SOD	20 ± 2	11 ± 3
CeO_2-SOD conjugate	12 ± 1	17 ± 2
CeO_2-SOD conjugate (3 h)	31 ± 1	40 ± 2

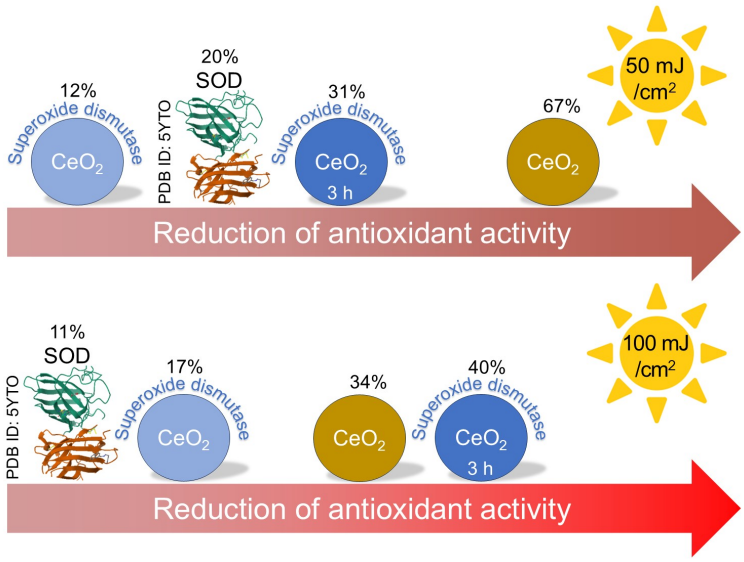

FIG. 5. Effects of UV irradiation on SOD-like activity of bare CeO_2 NPs, SOD and CeO_2-SOD conjugates

The antioxidant activity of the non-incubated CeO_2-SOD conjugate was reduced in a lesser degree under 50 mJ/cm^2 UV dose than under a 100 mJ/cm^2 dose, and their antioxidant activity was reduced to a lesser extent than that of the individual enzyme (Fig. 4(b), Table 1, Fig. 5). These results suggest that CeO_2 NPs exert a photoprotective effect towards the conjugated SOD, enhancing the operational stability of the conjugated enzyme under oxidative stress. Numerous studies have reported pronounced photoprotective properties of nanoscale CeO_2 [33, 50–52]. These protective effects are most commonly attributed to a combination of two key mechanisms: the ability of CeO_2 NPs to effectively absorb UV radiation and to mimic the functions of antioxidant enzymes, such as SOD and catalase, thereby reducing levels of ROS formed under UV exposure. It has been demonstrated that the photodegradation of organic dyes such as methyl orange [33], crystal violet [50] and rhodamine 6G [51] in the presence of CeO_2 nanoparticles is significantly lower than in the presence of conventional photocatalysts such as titanium dioxide [50].

The immobilized SOD enzyme efficiently attracts superoxide anion radicals to the nanoparticle surface due to its high affinity for this substrate [53, 54]. This dramatically increases the local concentration of superoxide anion radicals around the nanoscale cerium oxide. Consequently, any radicals that have not reacted with the SOD active site can be efficiently scavenged by the CeO_2 NPs. This process establishes a synergistic antioxidant cascade, in which the products of one reaction become the substrates for the next reaction.

The CeO_2-SOD conjugate aged for 3 h prior to irradiation showed a more pronounced reduction in SOD antioxidant activity after UV-irradiation with 50 mJ/cm^2 and 100 mJ/cm^2 doses (Fig. 4(b), Table 1, Fig. 5). This effect is presumably

attributed to substantial conformational changes in the SOD enzyme during the 3-hour incubation with CeO_2 NPs which could make the enzyme susceptible to UV-induced damage. Thus, the catalytic activity of the CeO_2-SOD conjugate under UV radiation depends not only on the properties of the CeO_2 NPs but also on the structure of the immobilized enzyme.

3.2.2. Prooxidant activity. The prooxidant activity of the samples was analyzed by monitoring chemiluminescence in the presence of luminol, a probe sensitive to hydrogen peroxide and reactive chlorine species [55, 56].

This study investigated the effect of UV irradiation on the redox behavior towards the hydrogen peroxide of bare CeO_2 NPs, individual HRP enzyme, and CeO_2-HRP conjugates, both immediately after mixing the components and after the incubation for 3 h. Fig. 6(a) shows chemiluminograms for the samples which were not subjected for UV-irradiation and the UV-irradiated samples. As can be seen, the analyzed samples enhance luminol-dependent chemiluminescence indicating the generation of ROS and supporting the prooxidant properties of the studied materials.

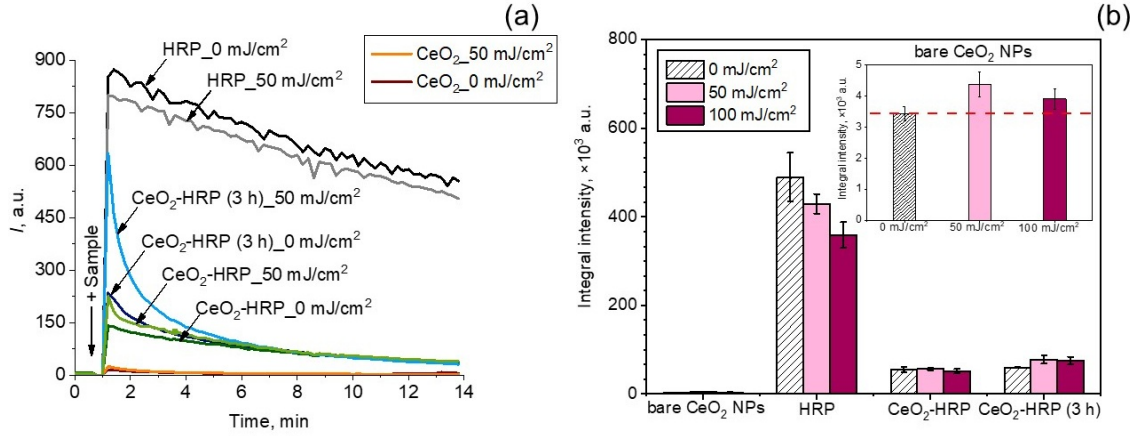

FIG. 6. (a) Chemiluminograms illustrating the prooxidant activity of bare CeO_2 NPs, HRP and CeO_2-HRP conjugates, (b) the light sums (prooxidant capacity) for the samples

From the chemiluminescence profiles, to quantify the prooxidant properties, the areas under the chemiluminescent curves (light sums) were calculated, which are proportional to the number of generated radicals and correspond to the prooxidant capacity of the samples. Fig. 6(b) shows the light sum bars. The most pronounced enhancement of the chemiluminescence signal was observed for the individual HRP enzyme. It should be noted that the shape of the chemiluminescent curve for the individual HRP differed from the experimental curves for other samples (Fig. 6(a)), which probably indicates different mechanisms of the prooxidant effect [20]. Analysis of the data (Fig. 6(b)) revealed that the CeO_2-HRP conjugates exhibited approximately 15 times higher prooxidant capacity compared to bare CeO_2 NPs. The increase in peroxidase-like activity is consistent with previous reports on hybrid nanobiocatalytic systems [57, 58]. For instance, the use of magnetite nanoparticles has been shown to significantly accelerate the hydrogen peroxide decomposition in the presence of HRP [58]. However, it is important to note that the HRP enzyme possessed lower activity upon the immobilization onto the CeO_2 nanoparticle surface (Fig. 6(b)). Presumably, this may also be caused by conformational changes in the enzyme structure and, as a result, steric hindrance to the access of the substrate to the active center.

To assess the effect of the UV radiation dose, the percentage decrease in the prooxidant activity of the analyzed materials was calculated (Table 2). For clarity, these data are also presented in Fig. 7.

A UV dose of 50 mJ/cm^2 enhanced the prooxidant activity of bare CeO_2 NPs more significantly than a dose of 100 mJ/cm^2 (Fig. 6(b)). In contrast, the activity of the native HRP enzyme decreased in a dose-dependent manner (Table 2), which is consistent with the recent reports [59, 60]. Notably, the CeO_2-HRP conjugate (obtained without pre-incubation) showed no significant change in activity after irradiation at 50 mJ/cm^2. Conversely, UV-irradiation with a

TABLE 2. Effects of UV irradiation on prooxidant activity of samples

Dose, mJ/cm^2	50	100
Sample	Reduction of prooxidant activity under UV irradiation, %	
Bare CeO_2 NPs	increase prooxidant activity	increase prooxidant activity
HRP	12 ± 5	27 ± 2
CeO_2-HRP conjugate	—	5 ± 1
CeO_2-HRP conjugate (3 h)	increase prooxidant activity	increase prooxidant activity

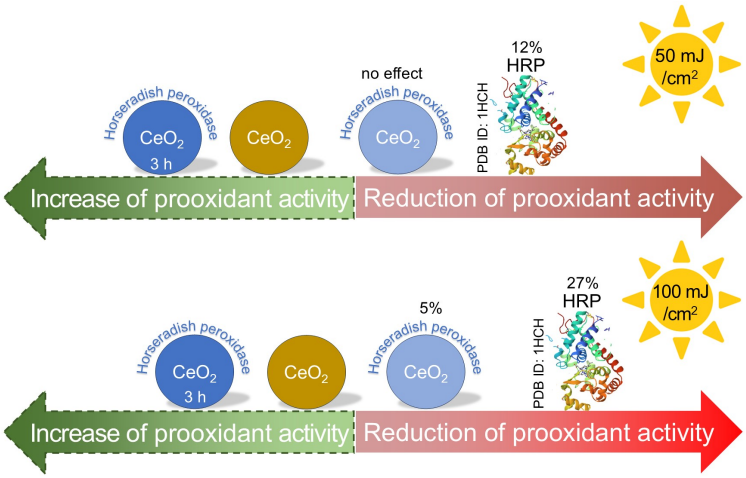

FIG. 7. Effects of UV irradiation on prooxidant activity of bare CeO_2 NPs, HRP and CeO_2-HRP conjugates

dose of 100 mJ/cm^2 resulted in a decrease in the activity. Compared to the native enzyme, the activity of HRP conjugated with CeO_2 (obtained without pre-incubation) did not change significantly under irradiation with a dose of 50 mJ/cm^2, and decreased to a lesser extent at 100 mJ/cm^2 (Table 2). These results could indicate a photoprotective effect of CeO_2 NPs toward HRP. This effect is probably due to the ability of CeO_2 NPs to effectively absorb UV radiation and thereby protect the protein molecule from direct photolytic damage.

Interestingly, for the CeO_2-HRP conjugate pre-incubated for 3 h, the UV-irradiation with both 50 and 100 mJ/cm^2 enhanced the peroxidase-like activity by an average factor of 1.5. This suggests that longer incubation promotes the formation of a more stable conjugate. Subsequent UV irradiation presumably modulates the redox properties of the nanoscale CeO_2 surface, creating more efficient synergistic catalysis – for instance, by facilitating electron transfer between the nanoparticle and the active site center of the enzyme.

4. Conclusions

The UV-tunable dual redox behavior of nanoscale CeO_2 and its hybrid materials with the SOD and HRP enzymes was studied. Bare CeO_2 NPs have been shown to possess SOD-like activity, which significantly reduced upon applying even low UV doses (50 mJ/cm^2). The CeO_2-SOD conjugates exhibited a 1.5-fold increase in the antioxidant activity compared to SOD alone. UV irradiation reduced the SOD-like activity of the hybrid materials, while CeO_2 NPs provided a pronounced photoprotective effect towards the enzyme.

In the presence of hydrogen peroxide, both bare CeO_2 NPs and their hybrids with HRP exhibited pronounced prooxidant properties, which can further be tuned by UV irradiation. The interaction of HRP with CeO_2 NPs resulted in the decrease of the activity of the enzyme however favored its stability under UV-irradiation.

These findings underscore the potential of nanoscale CeO_2 and its hybrids in biomedicine and catalysis, where external factors (e.g., via UV exposure) could alter the redox properties of the material. The methodology proposed in this study can be extended to the other models of oxidative stress, such as exposure to ultrasound, X-ray radiation, or radio waves.

References

[1] Mishra P., Lee J., Kumar D., et al. Engineered nanoenzymes with multifunctional properties for next-generation biological and environmental applications. *Adv. Funct. Mater.*, 2022, **32** (1), 2108650.
[2] Ma Y., Tian Z., Zhai W., Qu Y. Insights on catalytic mechanism of CeO_2 as multiple nanozymes. *Nano Res.*, 2022, **15** (10), P. 10328–10342.
[3] Thakur N., Manna P., Das J. Synthesis and biomedical applications of nanoceria, a redox active nanoparticle. *J. Nanobiotechnol.*, 2019, **17** (1), 84.
[4] Ilhan H., Ayvaz M.C. Evaluation of enzyme activity with nanoparticles conjugation. *Recent Adv. Mol. Biol. Biochem.*, 2023, 223.
[5] Gil D., Rodriguez J., Ward B., et al. Antioxidant activity of SOD and catalase conjugated with nanocrystalline ceria. *Bioengineering*, 2017, **4** (1), 18.
[6] Ding S., Cargill A.A., Medintz I.L., et al. Increasing the activity of immobilized enzymes with nanoparticle conjugation. *Curr. Opin. Biotechnol.*, 2015, **34**, P. 242–250.
[7] Ahmad R., Sardar M. Enzyme immobilization: An overview on nanoparticles as immobilization matrix. *Biochem. Anal. Biochem.*, 2015, **4** (1), 1.
[8] Sozarukova M.M., Proskurnina E.V., Mikheev I.V., et al. Anti- and prooxidant properties of cerium oxide nanoparticles functionalized with gallic acid. *Russ. J. Inorg. Chem.*, 2023, **68** (10), P. 1108–1116.
[9] Sozarukova M.M., Proskurnina E.V., Baranchikov A.E., Ivanov V.K. Antioxidant activity of conjugates of cerium dioxide nanoparticles with human serum albumin isolated from biological fluids. *Russ. J. Inorg. Chem.*, 2023, **68** (10), P. 1495–1502.
[10] Lasala P., Latronico T., Mattia U., et al. Enhancing antioxidants performance of ceria nanoparticles in biological environment via surface engineering with o-quinone functionalities. *Antioxidants*, 2025, **14** (6), 916.

[11] Pudlarz A.M., Czechowska E., Karbownik M.S., et al. The effect of immobilized antioxidant enzymes on the oxidative stress in UV-irradiated rat skin. *Nanomedicine*, 2020, **15** (1), P. 23–39.
[12] Sozarukova M.M., Kochneva E.M., Proskurnina E.V., et al. Albumin retains its transport function after interaction with cerium dioxide nanoparticles. *ACS Biomater. Sci. Eng.*, 2023, **9** (12), P. 6759–6772.
[13] McCord J.M. The evolution of free radicals and oxidative stress. *Am. J. Med.*, 2000, **108** (6), P. 652–659.
[14] Hensley K., Robinson K.A., Gabbita S.P., et al. Reactive oxygen species, cell signaling, and cell injury. *Free Radic. Biol. Med.*, 2000, **28** (10), P. 1456–1462.
[15] Chen D., Ai X., Li Y., et al. Protective effects of Cu/Zn-SOD and Mn-SOD on UVC radiation-induced damage in NIH/3T3 cells and murine skin. *Acta Histochem.*, 2023, **125**, 152030.
[16] Baldim V., Bedioui F., Mignet N., et al. The enzyme-like catalytic activity of cerium oxide nanoparticles and its dependency on Ce^{3+} surface area concentration. *Nanoscale*, 2018, **10** (14), P. 6971–6980.
[17] Heckert E.G., Karakoti A.S., Seal S., et al. The role of cerium redox state in the SOD mimetic activity of nanoceria. *Biomaterials*, 2008, **29** (18), P. 2705–2709.
[18] Sozarukova M.M., Shestakova M.A., Teplonogova M.A., et al. Quantification of free radical scavenging properties and SOD-like activity of cerium dioxide nanoparticles in biochemical models. *Russ. J. Inorg. Chem.*, 2020, **65** (4), P. 597–605.
[19] Korsvik C., Patil S., Seal S., et al. Superoxide dismutase mimetic properties exhibited by vacancy engineered ceria nanoparticles. *Chem. Commun.*, 2007, P. 1056–1058.
[20] Sozarukova M.M., Kozlova T.O., Beshkareva T.S., et al. Gadolinium doping modulates the enzyme-like activity and radical-scavenging properties of CeO_2 nanoparticles. *Nanomaterials*, 2024, **14** (5), 769.
[21] Shi X., Yang J., Wen X., et al. Oxygen vacancy enhanced biomimetic superoxide dismutase activity of CeO_2-Gd nanozymes. *J. Rare Earths*, 2021, **39** (10), P. 1108–1116.
[22] Li Y., He X., Yin J.J., et al. Acquired superoxide-scavenging ability of ceria nanoparticles. *Angew. Chem. Int. Ed.*, 2015, **54** (7), P. 1852–1855.
[23] Zhu A., Sun K., Petty H.R. Titanium doping reduces superoxide dismutase activity, but not oxidase activity, of catalytic CeO_2 nanoparticles. *Inorg. Chem. Commun.*, 2012, **15** (2), P. 235–237.
[24] Yadav N., Singh S. Polyoxometalate-mediated vacancy-engineered cerium oxide nanoparticles exhibiting controlled biological enzyme-mimicking activities. *Inorg. Chem.*, 2021, **60** (15), P. 7475–7489.
[25] Baranchikov A.E., Sozarukova M.M., Mikheev I.V., et al. Biocompatible ligands modulate nanozyme activity of CeO_2 nanoparticles. *New J. Chem.*, 2023, **47** (52), P. 20388–20404.
[26] Damle M.A., Jakhade A.P., Chikate R.C. Modulating pro- and antioxidant activities of nanoengineered cerium dioxide nanoparticles against *Escherichia coli*. *ACS Omega*, 2019, **4** (3), P. 3761–3771.
[27] McCormack R.N., Mendez P., Barkam S., et al. Inhibition of nanoceria's catalytic activity due to Ce^{3+} site-specific interaction with phosphate ions. *J. Phys. Chem. C*, 2014, **118** (33), P. 18992–19006.
[28] Xu C., Qu X. Cerium oxide nanoparticle: A remarkably versatile rare earth nanomaterial for biological applications. *NPG Asia Mater.*, 2014, **6** (3), e90.
[29] Alpaslan E., Geilich B.M., Yazici H., et al. pH-controlled cerium oxide nanoparticle inhibition of both gram-positive and gram-negative bacteria growth. *Sci. Rep.*, 2017, **7** (1), 45859.
[30] Pandey S., Kumari S., Manohar Aeshala L., et al. Investigating temperature variability on antioxidative behavior of synthesized cerium oxide nanoparticle for potential biomedical application. *J. Biomater. Appl.*, 2024, **38** (7), P. 866–874.
[31] Sozarukova M.M., Proskurnina E.V., Baranchikov A.E., et al. CeO_2 nanoparticles as free radical regulators in biological systems. *Nanosyst.: Phys. Chem. Math.*, 2020, **11** (3), P. 324–332.
[32] Klochkov V., Malyukin Y.V., Grygorova G., et al. Oxidation-reduction processes in CeO_{2-x} nanocrystals under UV irradiation. *J. Photochem. Photobiol. A Chem.*, 2018, **364**, P. 282–287.
[33] Zholobak N., Ivanov V., Shcherbakov A., et al. UV-shielding property, photocatalytic activity and photocytotoxicity of ceria colloid solutions. *J. Photochem. Photobiol. B Biol.*, 2011, **102** (1), P. 32–38.
[34] Wenk J., Brenneisen P., Meewes C., et al. UV-induced oxidative stress and photoaging. *Curr. Probl. Dermatol.*, 2001, **29**, P. 83–94.
[35] Pattison D.I., Rahmanto A.S., Davies M.J. Photo-oxidation of proteins. *Photochem. Photobiol. Sci.*, 2012, **11** (1), P. 38–53.
[36] Sozarukova M.M., Skachko N.A., Chilikina P.A., et al. Effect of low-dose line-spectrum and full-spectrum UV on major humoral components of human blood. *Molecules*, 2023, **28** (12), 4646.
[37] Plakhova T.V., Romanchuk A.Y., Butorin S.M., et al. Towards the surface hydroxyl species in CeO_2 nanoparticles. *Nanoscale*, 2019, **11** (43), P. 18142–18149.
[38] Madaeni S., Ghaemi N., Alizadeh A., et al. Influence of photo-induced superhydrophilicity of titanium dioxide nanoparticles on the anti-fouling performance of ultrafiltration membranes. *Appl. Surf. Sci.*, 2011, **257** (15), P. 6175–6180.
[39] Jimmy C.Y., Yu J., Ho W., Zhao, J. Light-induced super-hydrophilicity and photocatalytic activity of mesoporous TiO_2 thin films. *J. Photochem. Photobiol. A Chem.*, 2002, **148** (2–3), P. 331–339.
[40] Shcherbakov A.B., Teplonogova M.A., Ivanova O.S., et al. Facile method for fabrication of surfactant-free concentrated CeO_2 sols. *Mater. Res. Express*, 2017, **4** (5), 055008.
[41] Liochev S.I., Fridovich I. Lucigenin as mediator of superoxide production: Revisited. *Free Radic. Biol. Med.*, 1998, **25** (9), P. 926–928.
[42] Afanas'ev I.B. Lucigenin chemiluminescence assay for superoxide detection. *Circ. Res.*, 2001, **89** (11), e46.
[43] Sozarukova M.M., Proskurnina E.V., Ivanov V.K. Prooxidant potential of CeO_2 nanoparticles towards hydrogen peroxide. *Nanosyst.: Phys. Chem. Math.*, 2021, **12** (3), P. 283–290.
[44] Huber R., Stoll S. Protein affinity for TiO_2 and CeO_2 manufactured nanoparticles. From ultra-pure water to biological media. *Colloids Surf. A*, 2018, **553**, P. 425–431.
[45] Sendra M., Volland M., Balbi T., et al. Cytotoxicity of CeO_2 nanoparticles using in vitro assay with Mytilus galloprovincialis hemocytes: Relevance of zeta potential, shape and biocorona formation. *Aquat. Toxicol.*, 2018, **200**, P. 13–20.
[46] Socrates G. *Infrared and raman characteristic group frequencies: Tables and charts*. John Wiley & Sons, Chichester, 2004, 368 p.
[47] Bellamy L.J. *The infra-red spectra of complex molecules*. Springer Science & Business Media, London, 2013, 433 p.
[48] Rokhsat E., Akhavan O. Improving the photocatalytic activity of graphene oxide/ZnO nanorod films by UV irradiation. *Appl. Surf. Sci.*, 2016, **371**, P. 590–595.
[49] Wu T.-S., Syu L.-Y., Lin C.-N., et al. Enhancement of catalytic activity by UV-light irradiation in CeO_2 nanocrystals. *Sci. Rep.*, 2019, **9** (1), 8018.
[50] Gil D.O., Dolgopolova E.A, Shekunova T.O., et al. Photoprotector properties of ceria-based solid solutions. *Nanosyst.: Phys. Chem. Math.*, 2013, **4** (1), P. 78–82. (In Russian).

[51] Calvache-Muñoz J., Rodríguez-Páez J.E. Removal of rhodamine 6G in the absence of UV radiation using ceria nanoparticles (CeO_2-NPs). *J. Environ. Chem. Eng.*, 2020, **8** (1), 103518.
[52] Zhang L., Jiang H., Selke M., Wang, X. Selective cytotoxicity effect of cerium oxide nanoparticles under UV irradiation. *J. Biomed. Nanotechnol.*, 2014, **10** (2), P. 278–286.
[53] Osman R., Basch H. On the mechanism of action of superoxide dismutase: A theoretical study. *J. Am. Chem. Soc.,* 1984, **106** (19), P. 5710–5714.
[54] Noodleman L., Lovell T., Han W.-G., et al. Quantum chemical studies of intermediates and reaction pathways in selected enzymes and catalytic synthetic systems. *Chem. Rev*., 2004, **104** (2), P. 459–508.
[55] Marquette C.A., Blum L.J. Applications of the luminol chemiluminescent reaction in analytical chemistry. *Anal. Bioanal. Chem.*, 2006, **385** (3), P. 546–554.
[56] Kobayashi H., Gil-Guzman E., Mahran A.M., et al. Quality control of reactive oxygen species measurement by luminol-dependent chemiluminescence assay. *J. Androl.*, 2001, **22** (4), P. 568–574.
[57] Gao L., Giglio K.M., Nelson J.L., et al. Ferromagnetic nanoparticles with peroxidase-like activity enhance the cleavage of biological macromolecules for biofilm elimination. *Nanoscale*, 2014, **6** (5), P. 2588–2593.
[58] Corgié S.C., Kahawong P., Duan X., et al. Self-assembled complexes of horseradish peroxidase with magnetic nanoparticles showing enhanced peroxidase activity. *Adv. Funct. Mater.*, 2012, **22** (9), P. 1940–1951.
[59] Neves-Petersen M.T., Klitgaard S., Carvalho A.S.L., et al. Photophysics and photochemistry of horseradish peroxidase A2 upon ultraviolet illumination. *Biophys. J.*, 2007, **92** (6), P. 2016–2027.
[60] Falguera V., Moulin A., Thevenet L., Ibarz A. Inactivation of peroxidase by ultraviolet–visible irradiation: Effect of pH and melanoidin content. *Food Bioprocess Technol.*, 2013, **6** (4), P. 3627–3633.

Submitted 29 October 2025; accepted 16 November 2025

Information about the authors:

Madina M. Sozarukova – Kurnakov Institute of General and Inorganic Chemistry of the Russian Academy of Sciences, Leninskii prospect 31, Moscow, 119991, Russia; ORCID 0000-0002-5868-4746; s_madinam@bk.ru

Arina D. Filippova – Kurnakov Institute of General and Inorganic Chemistry of the Russian Academy of Sciences, Leninskii prospect 31, Moscow, 119991, Russia; ORCID 0000-0002-2725-8891; arifilippova@yandex.ru

Daria-Maria V. Ratova – Analytical Chemistry Division, Chemistry Department, M. V. Lomonosov Moscow State University, d. 1, Str. 3, Lenin Hills, GSP-1, Moscow, 119234, Russia; ORCID 0009-0006-0606-8059; darmarrat@gmail.com

Ivan V. Mikheev – Analytical Chemistry Division, Chemistry Department, M. V. Lomonosov Moscow State University, d. 1, Str. 3, Lenin Hills, GSP-1, Moscow, 119234, Russia; ORCID 0000-0002-2383-1697; mikheev.ivan@gmail.com

Elena V. Proskurnina – Kurnakov Institute of General and Inorganic Chemistry of the Russian Academy of Sciences, Leninskii prospect 31, Moscow, 119991, Russia; ORCID 0000-0002-8243-6339; proskurnina@gmail.com

Alexander E. Baranchikov – Kurnakov Institute of General and Inorganic Chemistry of the Russian Academy of Sciences, Leninskii prospect 31, Moscow, 119991, Russia; ORCID 0000-0002-2378-7446; a.baranchikov@yandex.ru

Vladimir K. Ivanov – Kurnakov Institute of General and Inorganic Chemistry of the Russian Academy of Sciences, Leninskii prospect 31, Moscow, 119991, Russia ORCID 0000-0003-2343-2140; van@igic.ras.ru

Conflict of interest: the authors declare no conflict of interest.